JOURNAL OF MATERIALS SCIENCE **38** (2003) 1231 – 1238

Effect of a machining-induced defect on the tensile strength of a 3D composite material

CATHERINE DAVY
Department of Engineering, University of Cambridge, Trumpington Street, Cambridge CB2 1PZ, UK
E-mail: cad41@eng.cam.ac.uk

DIDIER MARQUIS
LMT Cachan, 61 avenue du Président Wilson, F-94235 Cachan, France
E-mail: didier.marquis@ifma.fr

This paper investigates the effect of finite specimen size upon the tensile failure of a tridirectional carbon-carbon composite along each reinforcement axis. Asymmetry in the position of load-bearing axial yarns across the cross-section is generated randomly by machining. This yields parasitic bending of the specimen, and thereby premature failure of the yarns subjected to the maximum bending stress. However, bending effects become negligible at final failure. Additionally, the composite failure strength σ_F is determined from the cross-sectional area of the actually load-bearing axial yarns, using both symmetrical and asymmetrical specimens. Results are in good agreement with previous work, and we show that the variability of σ_F is small.

1. Introduction

Tridirectional carbon-carbon composites (3D C-C) are especially designed for high temperatures applications [1, 2]: they keep their mechanical properties at temperatures above 3000°C, outperforming any other material. Early experimental studies on 3D C-Cs have focused on processing effects upon composite microstructure and thermomechanical behaviour [3–9]. Various damage and failure models are also available [10–15]. 3D C-Cs damage up to failure under tensile off-axis or shear loading and under compressive loading [13, 15]. On the contrary, under tension along one or several reinforcement axes, failure prediction is based on the following Rankine-type criterion: a brittle-type failure occurs when ultimate strength is reached along any reinforcement axis [13, 15]. However, regarding tensile failure along a reinforcement axis, previous studies have not provided satisfactory answers to several key questions, as follows. 3D C-Cs are not notch sensitive: crack propagation due to an artificial notch does not induce failure [15]. So what is the cause of 3D C-Cs tensile failure along a reinforcement axis? Can an initial (as opposed to machined) microcrack or microvoid propagate through the entire composite and induce failure? Or does it rather correspond to the failure of load-bearing axial yarns? These composites are used in small structures (regarding their unit cell size) such as bolts and rivets [10]. Hence it is vital to ensure that 3D C-Cs are not sensitive to machining defects such as the partial cutting of load-bearing yarns. In small 3D C-C structures, can premature failure be induced by the reduction of some yarns cross-sectional area (due to their partial machining along their axis)? Moreover, brittle materials usually exhibit noticeable variability of their failure strength [16]: what is its extent for a 3D C-C? 3D C-C yarns are usually made of several thousand fibers, each exhibiting a noticeable variability of its failure strength [17]. In that case, Hild *et al.* [18] predict a deterministic axial tensile strength for each yarn, hence for the 3D C-C. Can this be experimentally proven? This paper addresses all of these questions as follows.

A description of the 3D C-C composite and the tensile test method is outlined in Section 2. In particular, the specimen cross-sectional area is equivalent to that of a bolt. Random machining of the specimen gives asymmetry in the position of axial yarns across the cross-section. This corresponds to a reduction of the cross-sectional area of several peripheral axial yarns. A total of 30 specimens is brought to failure so as to evaluate the failure strength variability. In Section 3, axial yarns breakage is identified as the main failure cause. Machining of yarns induces parasitic bending and premature breakage of greatly machined yarns. However, final failure is due to pure tensile loading for all specimens. A scheme is proposed to evaluate the composite failure strength σ_F along each reinforcement axis from symmetrical as well as asymmetrical specimens: σ_F is set by the cross-sectional area of all the actually resisting axial yarns. This allows to use all of our 30 tests to determine the associated scatter on σ_F, which is proven to be negligible. Concluding remarks are proposed in Section 4.

2. Experimental

This section details the 3D C-C architecture. Testing precautions and methodology follow.

2.1. Description of the material

We focus on a tridirectional carbon-carbon composite, see Fig. 1a. It is made of PAN-based carbon yarns impregnated with pitch-based carbon matrix. Its architecture is identical to Aérolor 32 manufactured by Aérospatiale (now part of EADS) [13], Fig. 1b. Continuous yarns are periodically disposed along three orthogonal directions of space denoted x, y and z, with the two yarn directions x and y being equivalent. Each x-axis (or y-axis) yarn is made of 6000 carbon fibres, whereas each z-axis yarn is made of 12000 carbon fibres. Reinforcement axes x, y and z are *orthotropy axes* for the material. Its unit cell is represented Fig. 2.

2.2. Experimental method

Several experimental difficulties arise when testing brittle materials. In particular, premature failure frequently occurs because of parasitic bending effects generated by, e.g., misalignments in the fastening heads [19]. To avoid this, we use a special set-up [20] equipped with Cardan joints that allow for rotation of each fastening head about two orthogonal axes, see Fig. 3a. In order

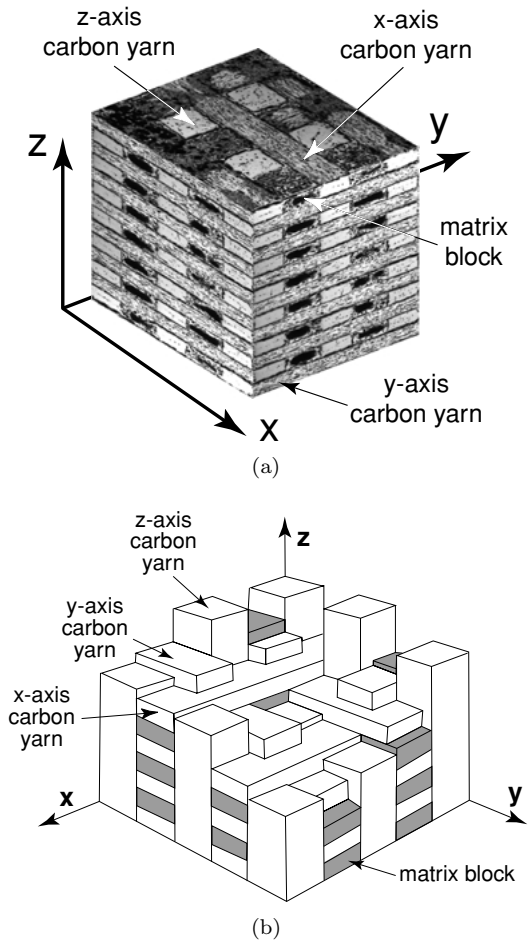

Figure 1 (a) The composite is made of continuous carbon yarns and carbon matrix. (b) Yarns are aligned in three orthogonal directions denoted x, y and z. Carbon matrix fills up the gaps, which are called *matrix blocks* [13].

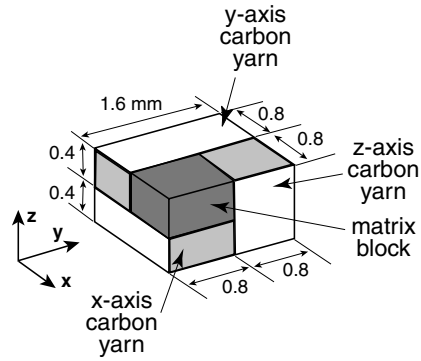

Figure 2 The composite unit cell: the composite entire architecture can be periodically reproduced in the 3D space by translating an elementary cell of $1.6 \times 1.6 \times 0.8\ \text{mm}^3$ [13]. The orthotropy (or reinforcement) axes x and y are equivalent: their yarns are of identical constitution and geometry, whereas those along the z-axis are twice the size of those along x or y. Two (1/8) portions of the cell are matrix-filled blocks.

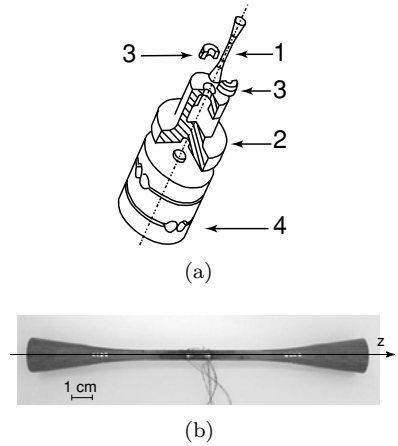

Figure 3 (a) Set-up [20] for brittle materials: a Cardan joint (4) allows rotation of the fastening head (2), thus limiting parasitic bending effects on the specimen (1). The specimen (1) is attached to the fastening head (2) using half-shells (3). (b) The geometry of a z-axis specimen (x-axis specimens are similar). Its cross-section represents 3×3 unit cells (resp. 3×6 unit cells for the x-axis geometry).

to validate the set-up, a 2017A specimen is tested and we show that it is actually subjected to a uniaxial pure tensile loading [21]. For all x- and z-axis specimens, Fig. 3b, the cross-sectional area is of similar size to a bolt and represents a few composite unit cells. More precisely, it is a multiple of the surface of that unit cell, displayed Fig. 2. Hence the specimen response is representative of the average response of the mesoconstituents (yarns and matrix blocks) [13]. For the same reason, the strain gauges size is a multiple of the elementary cell surface [22], and special care is taken for the gauges placement, as explained in [23]. Each specimen is equipped with four axial gauges, see Fig. 4. Besides, the axial yarns distribution is randomised by machining, see Fig. 5: specimens can have intact as well as randomly machined yarns, as displayed in Figs 4, 6a and b. The cross-sectional area of each deteriorated axial yarn is reduced to a given constant amount all along the specimen useful part. A total of 30 specimens is tested, with 20 specimens designed to test the z yarn direction (denoted $A1, \ldots, A20$), and 10 specimens designed to test the x (or equivalently y) yarn direction (denoted

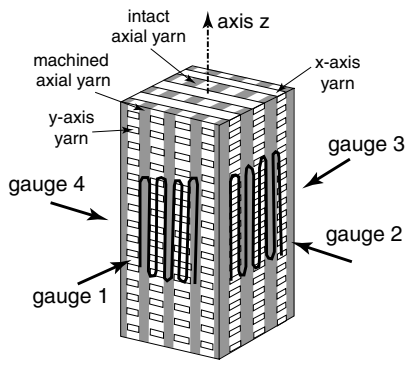

Figure 4 Location of axial gauges on a typical specimen. An asymmetrical axial yarns distribution is also shown: machined and intact axial yarns (in grey) are visible either at the edge or in the bulk of the specimen. Their distribution is similar to that of z-axis specimen $A1$.

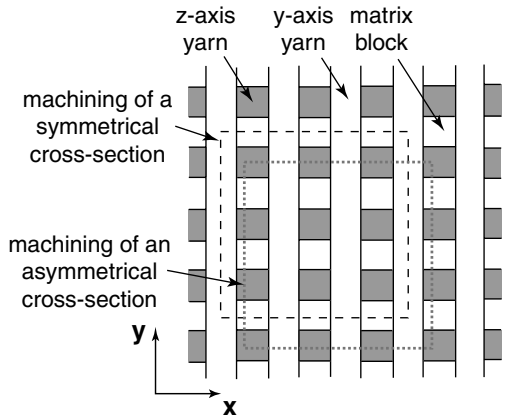

Figure 5 Random machining of z-axis tensile specimens (the technique is similar for x-axis specimens). The cross-sectional area is of fixed dimensions but its position in the (x,y) plane varies randomly from one specimen to another.

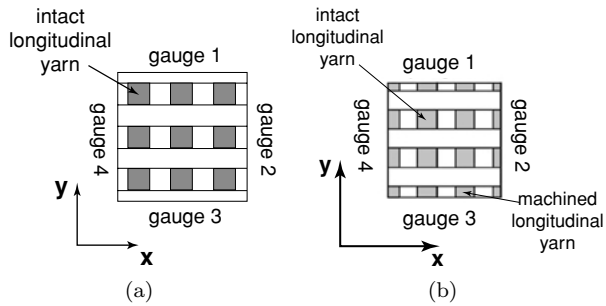

Figure 6 (a) Cross-section of a typical symmetrical specimen, named $A18$, and location of its strain gauges. (b) Cross-section of a typical asymmetrical specimen, named $A1$ and location of its strain gauges.

$XA1, \ldots, XA10$). Apart from $A7, A16, \ldots, A20$, all other specimens have an asymmetrical yarns distribution, which is associated to machined axial yarns, see Table I. During each test, series of loadings and unloadings are performed every 1000 N until specimen failure.

3. Results and discussion

In this section, the major influence of axial yarns on specimen tensile failure is shown. This helps understand the different failure mechanisms of either symmetrical or asymmetrical specimens. From this analysis, we evaluate the composite tensile strength σ_F along each orthotropy axis. Being a material characteristic, σ_F has to be independent of machining defects: a scheme to deduce σ_F from both symmetrical and asymmetrical specimens is proposed. Since a large number of specimens is brought to failure, see Table I (20 z-axis specimens), the variability of σ_F is also determined.

TABLE I Main results and characteristics of the 20 tests performed along axis z (those for the 10 specimens along axis x are similar)

Specimen name	Failure load (N)	Nb. of intact yarns	Nb. of machined yarns	Nb. × percentage of machined yarns (%)
$A1$	3646	4	12	[4 × 40, 4 × 60, 1 × 64, 2 × 76, 1 × 84]
$A2$	5382	6	6	[3 × 17.5, 3 × 92.5]
$A3$	3949	4	12	[2 × 18.7, 2 × 37.5, 1 × 49.2, 2 × 56, 1 × 64.5, 2 × 87.5, 1 × 92.2, 1 × 94.5]
$A4$	4623	4	8	[2 × 9.4, 2 × 31.3, 1 × 37.7, 2 × 81.3, 1 × 83]
$A5$	3853	4	12	[2 × 37.5, 2 × 50, 2 × 56, 1 × 68.7, 2 × 75, 1 × 78.1, 1 × 84.4, 1 × 89.1]
$A6$	4903	6	6	[3 × 21.9, 3 × 75]
$A7$	5340	9	0	–
$A8$	4568	4	8	[2 × 6.3, 2 × 37.5, 1 × 41, 2 × 56.3, 1 × 59]
$A9$	4840	6	6	[3 × 44, 3 × 69]
$A10$	5344	6	3	[3 × 6.3]
$A11$	4664	6	6	[3 × 44, 3 × 56]
$A12$	5978	9	0	–
$A13$	3942	6	6	[3 × 43.8, 3 × 66.3]
$A14$	5277	6	0	–
$A15$	4693	6	6	[3 × 3.8, 3 × 98.8]
$A16$	6209	9	0	–
$A17$	5979	9	0	–
$A18$	6268	9	0	–
$A19$	6327	9	0	–
$A20$	6264	9	0	–

3.1. Influence of axial yarns upon failure

The stiffness of a 3D C-C composite along each orthotropy axis is mainly that of the yarns located along that direction (Voigt approximation) [11]: $E_{zz} \approx f \times E_{z\text{-axis yarns}}$, where $E_{z\text{-axis yarns}}$ is the z-axis yarns Young's modulus and f is the portion of cross-section occupied by the yarns (yarns surface fraction). In other words, axial yarns sustain the main part of the load. Moreover, our post-mortem analyses show that tensile failure is also dictated by axial yarns. In Fig. 7, light microscopy and scanning electron microscopy photographs of specimen $A1$ are displayed. An uneven failure profile is clearly visible for each axial yarn, as well as a flat failure surface of the transverse part. This is typical of a yarn-dominated failure at the macroscopic specimen scale [24]: no crack from the transverse part has induced failure of the yarn (otherwise the failure surface would be continuing its progression inside the yarns). Instead, each carbon fibre has broken at its weakest point (thus explaining the uneven fibre-dominated profile of each yarn), yielding the

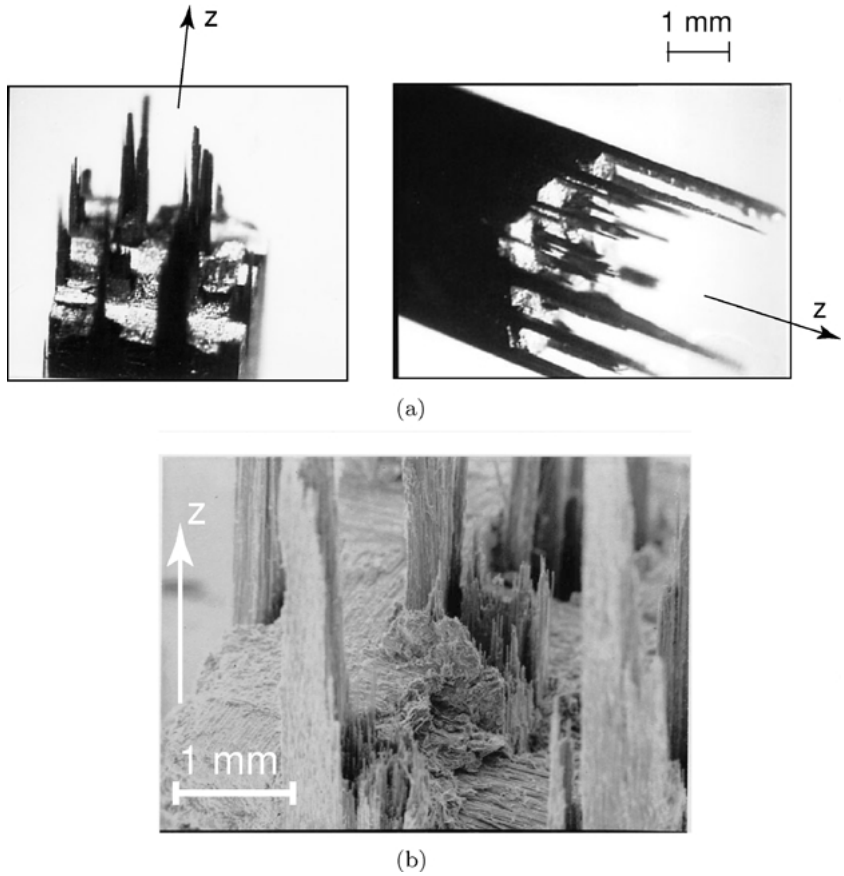

Figure 7 Specimen *A*1. (a) A *post mortem* photographs show significant pull-out of axial yarns. (b) SEM photograph of the failure surface shows the uneven failure of each axial yarn along with the flat failure profile of the transverse part.

overall specimen failure. These elements are essential for the understanding of the two failure mechanisms of typical intact yarns and machined yarns specimens.

3.2. Observed failure mechanisms

We mainly report on z-axis testing, as failure mechanisms are similar for x- (and y-) axis. Two main mechanisms are observed: they are described through the example of two typical specimens, symmetrical specimen *A*18 and asymmetrical specimen *A*1.

The first failure scenario concerns specimens with a symmetrical axial yarns distribution (i.e., specimens with symmetrical intact yarns only), such as *A*18, Fig. 6a. A typical elastic, linear and brittle behaviour is identified [13, 15]. More precisely, no parasitic bending effect is noticed on the gauge responses, see Fig. 8,

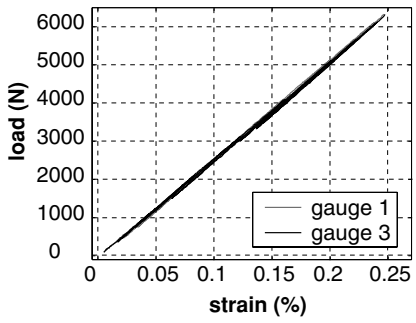

Figure 8 Typical gauge response for symmetrical specimen *A*18. Its behaviour is elastic, linear and its failure is brittle as shown in the case of gauges 1 and 3. Series of loadings and unloadings are performed every 1000 N until specimen failure.

which confirms that failure is caused by pure tensile loading and, as seen above, it corresponds to the failure of axial yarns.

On the contrary, specimens with an asymmetrical yarns distribution, such as *A*1, Fig. 6b, have a much different and unpredicted failure mode: they usually get damaged before final failure occurs (second failure scenario). This damage is attributed to the premature failure of greatly machined axial yarns. In Figs 9a and b, load remains constant (at 3300 N and 3500 N) whereas strain responses of gauges 1 and 2 decrease abruptly. This does not happen for gauges 3 and 4. We explain this phenomenon as follows. Gauges 1 and 2 are glued on greatly machined yarns (as opposed to gauges 3 and 4) which break at loads 3300 N and 3500 N. The load formerly sustained by those yarns is redistributed among the remaining axial yarns, whereas the deformation of broken yarns drops dramatically. Among all the specimens, this phenomenon is observed for every gauge glued on greatly machined yarns, which confirms the above explaination. Final failure of the specimen occurs when intact and slightly machined axial yarns break simultaneously at each fiber weakest point.

We now explain why greatly machined yarns break prematurely. Since the axial yarns distribution is not symmetrical, the specimen neutral axis does not coincide with its geometrical axis, thus causing bending. (Note that this parasitic bending effect is not caused by experimental artifacts, but rather by the specimen itself: it does not occur with 2017A or symmetrical composite

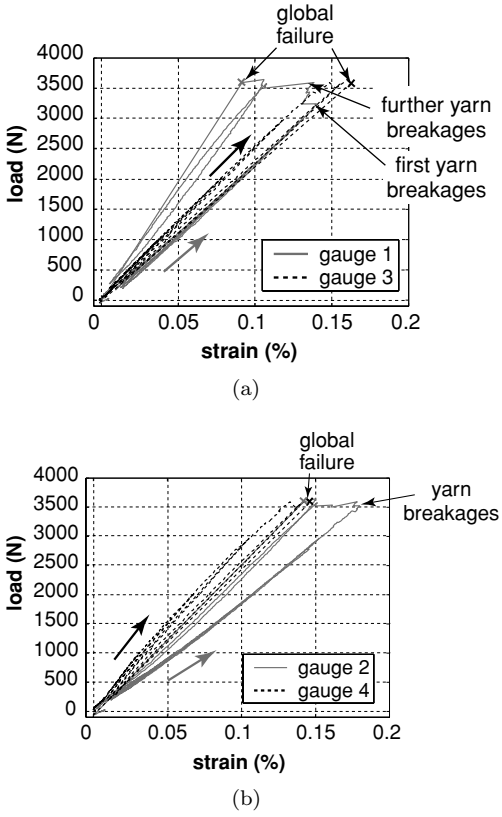

Figure 9 Typical gauge response for asymmetrical specimen $A1$. (a) Load vs. strain for gauges 1 and 3. $A1$ exhibits damage long before its overall failure, which is due to the failure of greatly machined axial yarns under gauge 1 (at 3300 N and 3500 N respectively). The arrows are along the direction of the initial elastic response. (b) Load vs. strain for gauges 2 and 4. Damage is also noticed on gauge 2 response at 3500 N. The arrows are along the direction of the initial elastic response.

specimens.) More precisely, the specimen dimensions being multiple of the elementary cell, when yarns on one side are machined at $\alpha\%$, with $\alpha \geq 50\%$, yarns located on the opposite side are machined at $(100-\alpha)\% \leq 50\%$. The cross-section bending centre is closer to the less machined yarns, see Fig. 10a. As a consequence, the most machined yarns are the most elongated, and they break before all the other yarns break.

For asymmetrical specimens, the set-up Cardan joints are generally not sufficient to fully eliminate bending until premature yarns breakage. In order to evaluate that bending effect, a specimen is modelled as an homogenised beam made of juxtaposed axial yarns. The bending effect is the semi-difference between the responses of gauges located on parallel sides of the specimen, see Fig. 10b. Although the bending effect between gauges 1 and 3 is of 5% only when machined yarns first break under gauge 1 at load 3300 N, it represents more than 15% between gauges 2 and 4 until load 3500 N is reached, when machined yarns located under gauges 1 and 2 break. The response of gauges located on greatly machined yarns can no more be considered valid after those yarns prematurely break. Yet their response is not zero: they mainly account for frictional effects between carbon fibres composing the broken yarns. Gauges 1 and 2 on specimen $A1$, see Fig. 9a and b, have indeed an hysteretical response after premature yarns breakage when the specimen is unloaded and then reloaded, which is attributed to friction between carbon fibres [18]. On the contrary, gauges 3 and 4 are valid up to global failure: they give an image of the behaviour of the yarns below them, and those do not break prematurely.

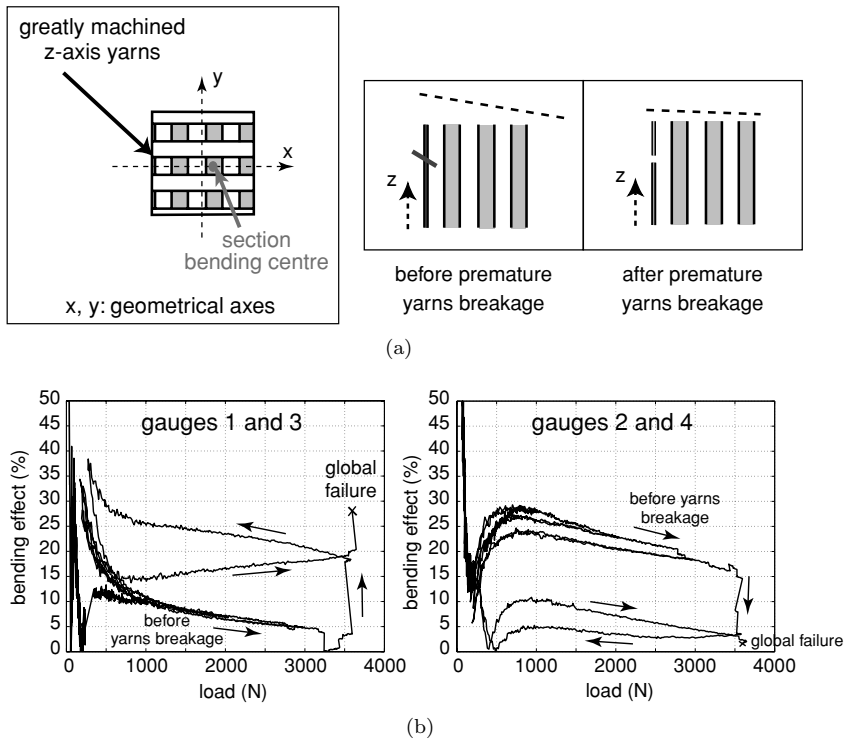

Figure 10 (a) Simple example of a specimen cross-section with asymmetrical yarn distribution along x-axis only. Due to the asymmetrical yarns distribution, the cross-section bending centre does not coincide with its geometrical centre, which causes parasitic bending. The specimen dimensions are chosen so that the less machined yarns are closer to the neutral axis. The most machined yarns are therefore the most elongated, and they break prematurely. After failure of greatly machined yarns, the specimen loading tends to reequilibrate and gets close to a tensile loading (cross-section normal to axis z). (b) Bending effect for specimen $A1$ evaluated as the semi-difference in gauges 1 and 3 response, and gauges 2 and 4 response (gauges on parallel opposite sides).

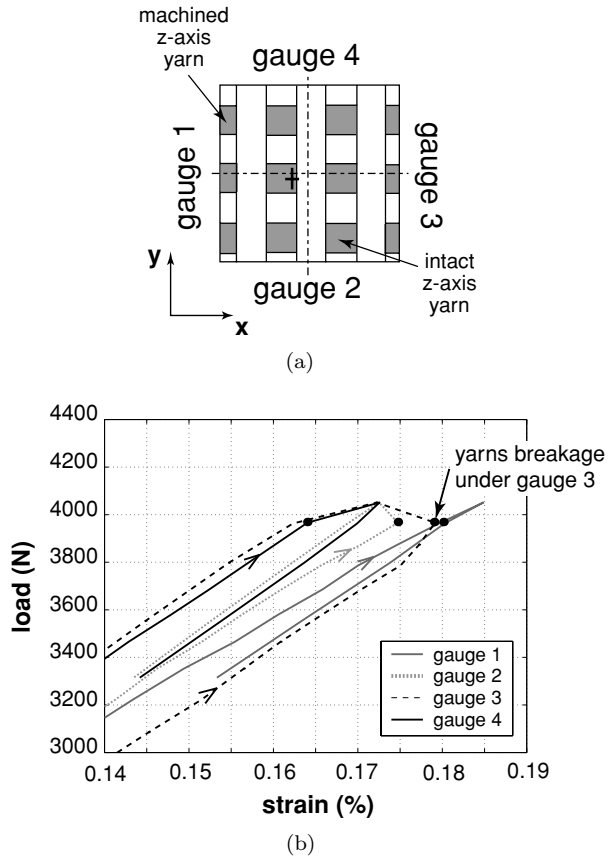

Figure 11 (a) Specimen $A11$ cross-section: its machined axial yarns (indicated in grey) are under gauges 1 and 3 only. The cross indicates the cross-section bending centre, which is not located on the dashed geometrical axes. (b) Close-up of $A11$ strain gauges response corresponding to yarns breakage under gauge 3. The loading direction is indicated by an arrow on each gauge response. The load corresponding to yarns breakage is indicated by a black dot on each gauge response.

After premature yarns breakages, the Cardan joints allow the specimen to reequilibrate and get under an almost pure tensile loading up to its global failure. Indeed, at final failure of $A1$, see Fig. 9a and b, gauges 3 and 4 which account for no damage have close responses (their difference represents 10% of their mean value and their slope is identical). Specimen $A11$ brings a better insight into this phenomenon. Its gauge responses are plotted Fig. 11b. This specimen has machined yarns on two sides only (under gauges 1 and 3), see Fig. 11a, and the specimen reequilibration is therefore more obvious than with $A1$: when yarns break prematurely under gauge 3, just below 4000 N, gauges 2 and 4 reequilibrate so as to give the same response. Simultaneously, gauge 1 increases its deformation. This shows that the specimen cross-section tends to get normal to the loading direction. Another convincing argument will arise in Subsection 3.4, where failure strength definition only takes pure tension into account. The variability characterising the failure strength is shown to be small: this would not be the case in the presence of parasitic bending.

3.3. Tensile failure strength along each orthotropy axis

Under pure uniaxial tension, failure strength is usually defined as the ratio of the failure load to the resisting cross-sectional area of the specimen [25]. This is not directly valid for 3D C-Cs because their main resisting constituents are the sole axial yarns. Here again, one can identify two cases.

- For symmetrical specimens, σ_F is simply defined as $f \times \frac{F_R}{S_{\text{yarns}}}$, where F_R is the failure load, S_{yarns} the intact axial yarns area and f is the yarns surface fraction (here equal to 25%). $\frac{F_R}{S_{\text{yarns}}}$ is indeed the average yarn failure strength, and is homogenised to the macroscopic scale using f [13]. This definition of σ_F is equivalent to $\frac{F_R}{S}$, where S is the specimen cross-sectional area.
- For asymmetrical specimens though, parasitic bending cannot be neglected during a great part of the test. In Subsection 3.2, we have explained that the specimen is very likely under pure tension after failure of greatly machined yarns. The above definition applies, with the greatly machined yarns being excluded however: S_{yarns} is the area of the intact and slightly machined yarns (also called *resisting* yarns).

Hence for asymmetrical specimens, one has to define precisely the resisting yarns cross-sectional area S_{yarns}. This comes down to determining which yarns actually resist, and which break prematurely. Recall that due to the choice of the specimen cross-section dimensions, when axial yarns are machined at $\alpha_1\%$ on side 1 (resp. $\alpha_2\%$ on side 2), then yarns located on the opposite side 3 (resp. on side 4) are machined at $\alpha_3 = 100 - \alpha_1\%$ (resp. $\alpha_4 = 100 - \alpha_2\%$). This results in bending, with the most machined yarns (i.e., those corresponding to the maximum value of either α_1 or α_3) being more elongated. The equilibrium situation corresponds to $\alpha_1 = \alpha_3 = 50\%$, therefore the edge value $\alpha_{\text{lim}} = 50\%$ determines which yarns break prematurely: if $\alpha_1 \leq \alpha_{\text{lim}}$ (the yarns are slightly machined on side 1), then the yarns located on side 3 break prematurely. If $\alpha_1 \geq \alpha_{\text{lim}}$ (the yarns are greatly machined on side 1), then the yarns located on side 1 break prematurely. The area S_{yarns} is then the total cross-section of intact yarns plus the total cross-section of yarns machined less than $\alpha_{\text{lim}} = 50\%$.

In order to ascertain this reasoning, we investigate statistical issues: the adequate value $\alpha_{\text{lim}} = 50\%$ is proven to correspond to the minimum variance on σ_F. For each specimen, the measured tensile failure strength $\sigma_{F\,\text{measured}}$ is evaluated as

$$\sigma_{F\,\text{measured}} = f \times \frac{F_R}{S_{\text{yarns}}(\alpha_{\text{lim}})}$$

where f is the surface fraction of axial yarns, F_R is the failure load and $S_{\text{yarns}}(\alpha_{\text{lim}})$ is the cross-sectional area of intact yarns plus that of yarns machined less than $\alpha_{\text{lim}}\%$. Let α_{lim} vary from 0% (intact yarns only) to 100% (all intact and machined yarns are taken into account). Therefore $\sigma_{F\,\text{measured}}$ depends on the intrinsic material failure strength $\sigma_{F\,\text{intrinsic}}$ (that can be random), and it also depends on errors due to an incorrect estimation of the resisting yarns cross-sectional area S_{yarns} (and it depends for a minor part on measurement

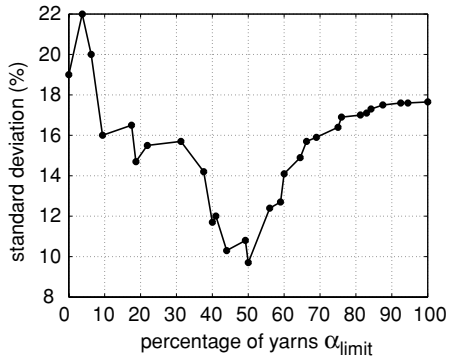

Figure 12 Standard deviation vs. $\alpha_{\lim}$ percentage of machined yarns taken into account to evaluate the average tensile failure strength σ_F along axis z.

errors). All of these errors are denoted $\varepsilon_{\text{area error}}$. More specifically, for each specimen,

$$\sigma_{F\,\text{measured}} = \sigma_{F\,\text{intrinsic}} + \varepsilon_{\text{area error}}$$

The variance composition theorem [26] yields (where Var$(\cdot)$ denotes the variance)

$$\text{Var}(\sigma_{F\,\text{measured}}) = \text{Var}(\sigma_{F\,\text{intrinsic}}) + \text{Var}(\varepsilon_{\text{area error}})$$

The most likely value of $\alpha_{\lim}$ is the one which minimises Var$(\varepsilon_{\text{area error}})$. The above relationship shows that it also corresponds to a minimum of Var$(\sigma_{F\,\text{measured}})$: the most likely value for $\alpha_{\lim}$ corresponds to a minimum value of the overall variance Var$(\sigma_{F\,\text{measured}})$. In Fig. 12, the standard deviation (square root of the variance Var$(\sigma_{F\,\text{measured}})$) is clearly minimum for $\alpha_{\lim} = 50\%$. This result is a statistical confirmation of the above physical explanation.

3.4. Variability of the tensile failure strength

Evaluation of the failure strength σ_F is performed for z-axis tests, as well as for x- (or equivalently y-) axis tests, and so is its variability. Scatter on failure strength is usually determined by either the standard deviation or the parameters of a two parameter Weibull law [16, 17, 27–29]. For typically dispersive materials, the first Weibull parameter m varies between 3 and 15, and the greater m, the less dispersive the material. The second Weibull parameter S_0 is interpreted as the failure stress corresponding to a failure probability of 63%.

Table II gives the average σ_F, its standard deviation and m for each orthotropy axis of our 3D C-C. In each case, the failure stress is computed as $\sigma_F = f \times \frac{F_R}{S_{\text{yarns}}}$, where S_{yarns} is the cross-sectional area taking into account all the yarns such that $\alpha \leq 50\%$.

For axis z, scatter is evaluated either with symmetrical specimens only ($m = 27$), or with symmetrical and asymmetrical specimens ($m = 12$): the composite has a deterministic behaviour only when symmetrical specimens are considered ($m > 15$). The difference is that when considering asymmetrical specimens, σ_F takes into account resisting but slightly machined yarns which induce an additional scatter. Indeed, though these yarns are only partially machined and resist up to the specimen overall failure, machining has made them more fragile and has randomised their actual strength. This phenomenon has a much smaller effect on x-axis scatter. All x-axis specimens have machined yarns, but their proportion is much lower than for z-axis specimens (this is due to the fact that x-axis yarns are two times smaller that-z axis yarns). For example, the typical asymmetrical z-axis specimen $A1$ has 4 machined yarns with $\alpha \leq 50\%$ and 4 intact yarns, see Fig. 6b. On the contrary, the typical asymmetrical x-axis specimen $XA1$ has only 7 machined yarns with $\alpha \leq 50\%$ and 10 intact yarns, see Fig. 13. As a consequence of this difference, the effect of slightly machined yarns on failure strength variability is smaller, yielding a negligible scatter ($m = 20$).

TABLE II Evaluation of tensile failure strengths of 3D C-C and associated scatter along axes x (or equivalently y) and z

Type of specimen	Failure stress σ_F (MPa)	Weibull parameter m (no unit)	Standard deviation (%)
z-axis (20 symmetrical and asymmetrical specimens)	241	12	8.8
z-axis (6 symmetrical specimens)	268	27	2.5
x-axis (10 asymmetrical specimens)	217	20	5

Finally, for z-axis specimens, the evaluation of σ_F is really representative of the sole composite behaviour when only symmetrical specimens are taken into account (specimen machining does not affect it), and we find $\sigma_{zz\,\lim} = 268$ MPa. For x-axis (and equivalently y-axis) specimens, machining effect is small enough so that all asymmetrical specimens are taken into account for the evaluation of the failure stress, and we find $\sigma_{xx\,\lim} = 217$ MPa. For both $\sigma_{zz\,\lim}$ and $\sigma_{xx\,\lim}$, the maximum standard deviation is 5% only. Note that our estimations of $\sigma_{zz\,\lim}$ and $\sigma_{xx\,\lim}$ are in good agreement with those in [13] for Aérolor 32. Moreover, we show that the associated scatter is small. This feature is explained as follows. 3D C-C failure is governed by axial yarns, which are themselves governed by fibres failure, see Subsection 3.1. At the microscopic scale, each fibre breaks at its weakest point, and studies have proven that its failure stress has a noticeable variability [17]. However, due to the great number of fibres a yarn comprises (between 6 and 12 thousands), the law of large numbers levels this dispersive behaviour, as predicted by [18]. We therefore identify a negligible scatter

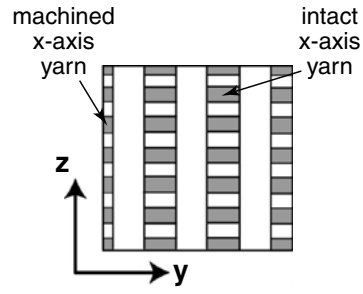

Figure 13 A typical x-axis specimen cross-section: $XA1$ cross-section comprises 11 axial yarns machined more than 50%, 7 axial yarns machined less than 50% and 10 intact yarns.

at the macroscopic scale of the specimen, though it is made of a tenth yarns only. In practice, this result means that even when considering small symmetrical 3D C-C structures, their tensile failure strength along a reinforcement axis is deterministic, and directly represents the material intrinsic failure strength. For small asymmetrical parts though, an additional scatter affects the structure tensile failure strength along a reinforcement axis, and this should be avoided. It is a direct consequence of the yarns machining, which affects even the very partially deteriorated ones.

4. Concluding remarks

A structure made of 3D C-C is typically designed to sustain tensile loadings along one (or several) of the composite reinforcement axes. This experimental study has brought better knowledge of 3D C-Cs failure mechanisms under tensile loading along a single reinforcement axis: stiffness as well as failure are both governed by the axial yarns. For completeness, the case of off-axis tensile failure or compressive failure have been tackled in [13, 15].

When a 3D C-C is used in small structures (of size similar to that of its unit cell), any machining defect affecting its yarns dramatically changes the tensile failure scenario. Without any machining defect (symmetrical structures), failure is tensile and brittle. On the contrary, an asymmetrical distribution of axial yarns generates parasitic bending. This causes premature damage (attributed to premature yarn failures) prior to final tensile failure. Additionally, a scheme evaluates the composite ultimate tensile strength σ_F using both symmetrical and asymmetrical specimens: σ_F is set by the cross-sectional area of all the actually resisting axial yarns (cross-sectional area machined less than $\alpha_{\lim} = 50\%$). This result is valid only when the proportion of slightly machined yarns does not induce scatter on σ_F: for our 3D C-C, it is only valid for axes x and y. The values for σ_F are in good agreement with previous work, and its variability is proven to be minor. It is concluded that, for small symmetrical 3D C-C structures subjected to a tensile loading along a reinforcement axis, the failure strength (and its corresponding negligible variability) is directly that of the composite. On the contrary, small asymmetrical parts should be avoided as machining defects cause additional scatter on the structure tensile failure strength.

Acknowledgments

The authors are grateful to Dr S. Calloch and Dr F. Hild for useful scientific discussion, and to Dr A. Cosculluela for following the project from its very beginning to its end. This work has been funded by Commissariat à l'Energie Atomique under contract no. CEA/LR/9T2265/CD.

References

1. A. LEGENDRE, Le matériau Carbone: des céramiques noires aux fibres de carbone (Eyrolles, 1992).
2. G. SAVAGE, Carbon-carbon Composites (Chapman and Hall, 1993).
3. D. F. ADAMS, *Mat. Sci. and Eng.* **23** (1976) 55.
4. J. S. BASTE and B. HOSTEN, *Rev. de Phys. Appl.* **25**(2) (1990) 161.
5. J. JORTNER, *Carbon* **24**(5) (1986) 603.
6. P. LARAMEE, G. LAMERE, B. PRESCOTT, R. MITCHELL, P. SOTTOSANTI and D. DAHLE, in "Proc. 12th Biennal Conf. on Carbon," *Am. Chem. Soc.* (Washington, DC, 1975) p. 74.
7. L. E. MCALLISTER and W. LACHMANN, edited by A. Kelly and S. T. Millieko (North Holland, 1983) p. 109.
8. J. L. PERRY and D. F. ADAMS, *Carbon* **14** (1976) 61.
9. J. L. WHITE and P. M. SHEAFFER, *Carbon* **27**(5) (1989) 697.
10. O. ALLIX, M. DOMMANGET, M. GRATTON and P. L. HEREIL, *Comp. Sci. and Tech.* **61**(3) (2001) 409.
11. O. ALLIX and P. LADEVEZE, in Advanced Composites Materials II, Leading Part for the XXIst Century, "Proceedings of the second Japan-France Joint Seminar on Composite Materials," Tsukuba, Japan, edited by C. Bathias and M. Uemara (SIRPE, Paris, 1991).
12. J. S. BASTE, C. CHARCOSSET and F. SIDOROFF, in "Compte-Rendus des 6èmes Journées Nationales sur les Composites" (AMAC, Paris, 1988) p. 765.
13. J. P. DUMONT, P. LADEVEZE, M. POSS and Y. REMOND, *Int. J. of Comp. Struct.* **8** (1987) 119.
14. S. IVANOV, A. A. TASHKINOV and V. P. SKACHKOV, in "Proc. of the 5th International Conference on Biaxial/Multiaxial Fatigue and Fracture" (Cracow, 1997) p. 267.
15. C. T. ROBINSON and P. H. FRANCIS, Fatigue of Fibrous Composite Materials, ASTM-STP 723 (American Society for Testing and Materials, 1981) p. 85.
16. F. HILD and D. MARQUIS, *Eur. J. of Mech. A/Solids* **11**(6) (1992) 753.
17. Y. TANABE, E. YASUDA and M. INAGAKI, *J. of Mat. Sci. Lett.* **10** (1991) 756.
18. F. HILD, A. BURR and F. A. LECKIE, *Eur. J. of Mech.—A/Solids* **13**(6) (1994) 731.
19. J. P. BOEHLER and L. EL AOUFI, in "Compte-rendus des Journées Nationales AMAC-GAMAC" (AMAC, Paris, 1989) p. 3.
20. F. HILD, French patent no. 90 06848 (Régie Nationale des Usines Renault—ENS de Cachan, 1992).
21. C. CRESTIA-DAVY, S. CALLOCH, A. COSCULLUELA, F. HILD and D. MARQUIS, in "Proc. of the 12th International Conference on Composite Materials" (Paris, July 1999).
22. P. LADEVEZE, Y. REMOND and E. VITTECOQ, *Rev. Franç. de Méc.* **2** (1989) 219.
23. R. J. WHITEHEAD, Technical Note NT. 205 (Vishay Micromesures MM, 1984).
24. R. J. ZALDIVAR, G. S. RELLICK and J.-M. YANG, *J. Am. Ceram. Soc.* **78**(3) (1995) 623.
25. M. F. ASHBY and D. R. H. JONES, Engineering Materials 1: An Introduction to Their Properties and Applications, 2nd ed. (Oxford, 1996).
26. M. L. BERENSON, D. M. LEVINE and D. RINDSKOPF, Applied Statistics: A First Course (Englewood Cliffs, NJ, 1988).
27. N. LISSART and J. LAMON, *J. of Mat. Sci.* **32**(22) (1997) 6107.
28. M. R'MILI and M. MURAT, *C. R. Acad. Sci. Paris—End. Fat. Rupt.* **324**(II b) (1997) 355.
29. W. WEIBULL, *Proc. Roy. Swed. Inst. Eng. Res.* **151/153** (1939).

Received 26 March
and accepted 29 October 2002